Macromolecules
ARTICLE

Macromolecules **2010**, *43*, 5881–5887 **5881**
DOI: 10.1021/ma100697v

Does Fractal Nanostructure of Filled Rubber Lead to Fractal Deformations? In Situ Measurements of Strain Heterogeneities by AFM

Olivier Lame*

INSA Lyon, MATEIS UMR 5510 20 av Albert Einstein 69621 Villeurbanne

Received March 31, 2010; Revised Manuscript Received May 18, 2010

ABSTRACT: The filler network in filled rubbers exhibits a very disordered structure which is close to a fractal pattern. During mechanical solicitation, the interaction between polymer and the filler network leads to local strong heterogeneous deformation. The question is: How does the fractal structure of the filler network affect these deformations? Direct observation of these microstructures, in particular under an imposed deformation, is difficult; however, AFM phase imaging can fulfill this objective. Local deformation of the filler networks has been observed in situ along two loading sequences. Fracture in the filler network has been observed, strong deformation heterogeneities have been measured. It has been also shown that, from the first loading to the second, the aggregates seem to follow the same path even if the strain heterogeneities increase. Finally, along a current line, the heterogeneities of deformation are self-similar until a maximum size is reached. This size has been determined to be approximately 1 μm, and the return to homogeneity does not occur before 50 μm.

Introduction

Mechanical properties of filled rubber are well-known to be related to the filler network and the interaction between fillers and rubber.[1−6] On a nanometric scale, strong heterogeneities of filler concentration (either carbon black or silica) lead to the formation of aggregates and agglomerates exhibiting a wide size distribution.[7] This complex microstructure is generally considered as a fractal network[8,9] as concentration heterogeneities are almost self-similar along a large range of scales. During loading, nonlinear behaviors such as Payne[10,11] and Mullins effects[12−14] occur due to filler structure rearrangement, partial break of the filler network and its interactions with rubber.[15,16] Modeling filled rubber mechanical properties requires taking into account this very specific microstructure. Some mechanical models have been proposed[17] in particular to take into account the fractal characteristics of the microstructure. However, their reliability and principally their correlation with local mechanisms could be improved. To reach this goal, major difficulties have to be faced. First the relation between the fractal microstructure and the mechanical response should be clarified. Does the deformations are also fractal and until which scale? In addition, the consequence on the local microstructure of the irreversible phenomena occurring after the first loadings (Mullins effect) should be evaluated.

It is particularly difficult to elucidate these latter questions because very few quantitative experimental data exist about the local evolution of the filler network along deformation cycles. In this paper, we propose to show how a meticulous analysis of tapping mode AFM images can bring new experimental clues concerning the relation between heterogeneous local behavior and the macroscopic one. Tapping mode AFM has been shown to be a powerful tool to observe at a nanoscale the filler network.[18−20] Indeed it allows discriminating the hard and soft phase on a nanometric scale.[21−25] A simple tension device allowing imposing a constant strain has been designed for AFM observations. In situ AFM scanning have been performed during the two first loading sequences until 120% of deformation on same zone. Then, movements of individual aggregates have been followed along the tensile test. This kind of experiment was initiated by Lapra et al.[26] and Christenson.[27] The questions of the influence of the macroscopic strain on the filler networks, the reversibility after a first loading will be addressed. The maximum characteristic size where the structure can be considered as fractal has been examined, as well as the size where the homogeneous behavior is recovered.

Experimental Section

The material chosen is a filled rubber composed with SBR (25 wt % of styrene, 55 wt % of 1,2-polybutadiene, and 20 wt % of 1,4-polybutadiene, without oil) provided by Bayer S.A. Then 15 phr of carbon black filler has been added (N234 provided by CABOT Corporation, with an average particle size of 24−29 nm and a specific surface of 124 m^2/g). The relatively low filler rate has been chosen to make easier the phase AFM observation. The material is therefore below the mechanical threshold and close to the electrical one.[28] Particularly flat films were prepared by compression molding between flat surfaces. Bone shaped samples are finally obtained with sizes of 0.5 mm thickness, 6 mm width, and 30 mm length.

Before imaging the material by AFM, a classical tensile test has been realized to evaluate the Mullins effect. The results observed on Figure 1 have shown that the first loading is significantly different from the following ones, but no significant difference is observed between the second and the third. Consequently the present study will be restrained to the first and the second loadings.

Concerning the AFM setup, A Veeco (Santa Barbara, CA) NanoScope Dimension 3100 was used in tapping mode with silicone cantilevers with resonance frequencies close to 350 kHz. The set point was modified at each deformation steps in order to maximize the phase contrast. To perform in situ AFM observation, an experimental device (Figure 2) has been designed. It is composed with a tension device located under the AFM cantilever. In the Figure 2, the AFM tip would be situated in place of

*Corresponding author. E-mail: Olivier.lame@insa-lyon.fr.

Published on Web 05/28/2010

the reader. The elongation is applied thanks to screws so that a constant strain can be applied to the sample. An adjustable sample table allows elevating slightly (less than 1 mm) the rubber film in order to maintain it on a rigid plane surface so that no vertical movement could perturb the scanning.

To observe the filler network deformation along the first and the second loading the following procedure has been used:

- A zone is chosen by optic microscopy where easily identifiable topographical incident can be seen (around 20 μm × 20 μm).
- Inside this zone, a lower size zone is chosen by AFM observation where easily identifiable aggregates can be seen (around 5 μm × 5 μm).
- AFM scanning is performed at different scales (three scan sizes have been chosen) on the same zone.
- Then the draw ratio is increased and the previous experiments are performed again (five draw ratios have been chosen).
- This procedure is repeated again for the second loading.

To sum up, for 0, 30, 60, 9,0 and 120% of draw ratio, three scan sizes (3 × 3, 5 × 5, and 7 × 7 μm) are realized for the first and the second loading. All the observations have been done on the same zone of the material. Finally, in order to obtain a stable image, all of the AFM scannings are performed 20 min after each elongation step.

Local strain is evaluated by measuring the distance between aggregates. Thanks to these numerous images, local deformation of the microstructure has been measured and compared to the macroscopic deformation.

A Preliminary Analysis. An example of the first loading course is presented in Figure 3.

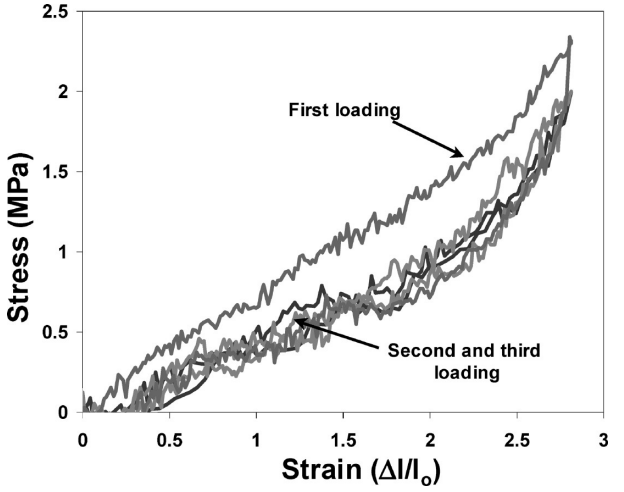

Figure 1. Stress/strain curves (3 cycles) of a 15 phr filled rubber.

The tensile axis is horizontal, and an easily identifiable aggregate is rounded all along the tensile test. First of all, it can be seen that during loading, "new aggregates" appear as if they emerge out of the material.[29] Moreover, the size and the contrast of the aggregates increase. These effects prevent us from using image correlation analysis software. The measurements have to be done "manually". Considering easily identifiable aggregates (an example is rounded on the Figure 3), it is possible to measure the local deformation in the tension direction and compare it to the macroscopic deformation. To evaluate strain heterogeneity, it has been decided to measure the relative elongation ε in the axial direction.

$$\varepsilon = \Delta l / l_o \quad (1)$$

Here, l_o is the initial size of the aggregate and Δl the size increase under loading.

This definition is not the rigorous strain for large Δl, but it is simple and enough to compare different zones. Δl, and l_o are measured between two aggregates and several zone of different initial size (initial spacing between aggregates) are chosen. As the measurements are performed directly on the images, a relative precision of around 10% is obtained.

Results

Filler Network Behavior in the Axial Direction. Topographical Evolution. As it has been seen on Figure 3, when the imposed macroscopic strain is increased, the aggregates seem to become more numerous, bigger and clearer. In fact by analyzing the topographical evolution for the extreme macroscopic strains, i.e., for 0 and 120%, (Figure 4), it appears that the roughness (or topography) increases strongly. Indeed, the height of the same line is reported at 0%, 120% and again 0% (after unloading). Under loading, only a fraction of the initial 3 μm length is represented. The maximum difference of height is around 160 nm, whereas it is only around 40 nm before and after loading. Comparing the initial curve with the one under loading, it can be seen that initial slight defect becomes under loading significant asperities. This observation is consistent

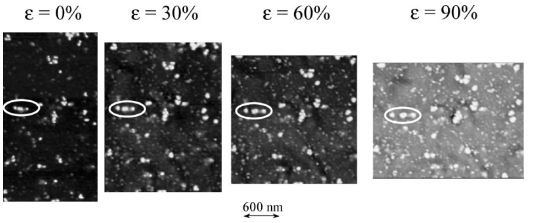

Figure 3. AFM phase images of the same zone realized at 0, 30, 60, 90% of macroscopic deformation.

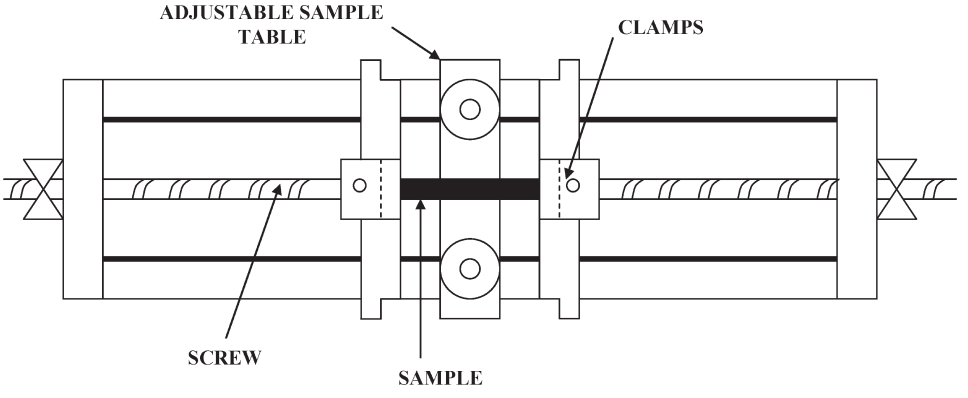

Figure 2. In situ tension device designed for AFM observations.

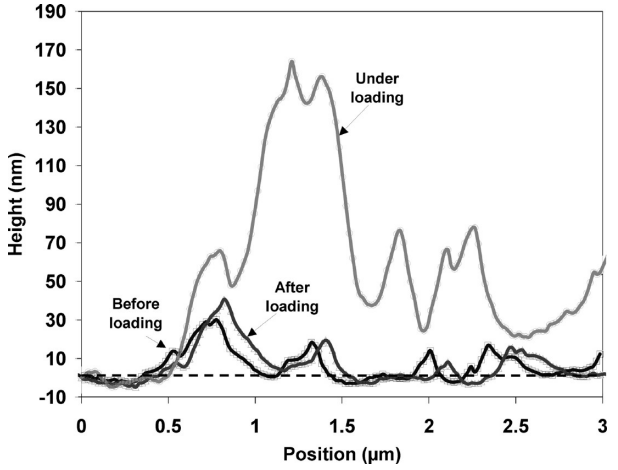

Figure 4. Topography on a 3 μm line before loading, during loading (120% strain) and after loading.

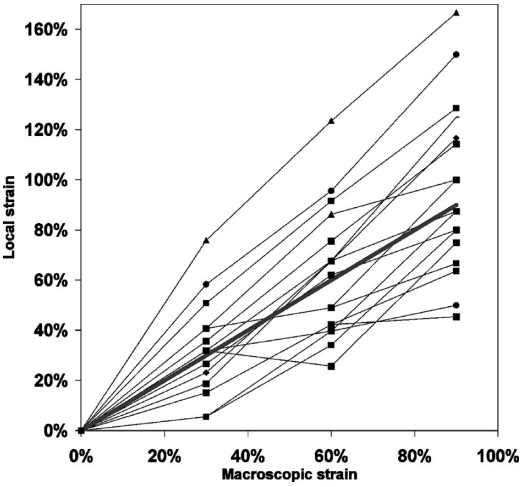

Figure 5. Relative elongation of several zones taken in 5 × 5 μm image size compared to the macroscopic relative elongation.

with the "appearance" of new filler on the images. It is worth noting that the topographical evolution is quasi reversible.

This effect has already been observed by Lapra.[29] There is no definitive explanation however it is plausible that the topographical increase would originate in the filler network resistance. Indeed, if only a part of the filler networks is brought with the rubber flow, some new aggregates could emerge on the surface as if a rigid skeleton of aggregates were kept undeformed in the direction perpendicular to the tensile one.

Filler Network Behavior in the Axial Direction. Strain Heterogeneity. Several zones of different initial size (initial gap between two aggregates) from 20 to 30 nm to around 2000 nm have been chosen, the deformation is measured in the tension direction. The intensity of strain heterogeneities is represented on the Figure 5. On this figure is plotted the local strain versus the macroscopic one. The continuous straight line represents the macroscopic strain and all the other curves represent the local deformation of the different zones measured by analyzing AFM phase image. As we can see, the gap between macroscopic and local strain increases for the higher macroscopic strain. Some zones exhibits always a lower strain whereas others exhibits always a higher strain which was an expected result as the material has to follow the imposed macroscopic strain. To quantify the strain heterogeneity intensity, the following ratio between local and macroscopic deformation can be considered:

$$\frac{|\varepsilon_0 - \varepsilon_{\text{local}}|}{\varepsilon_0} = \frac{|\Delta\varepsilon|}{\varepsilon_0} \qquad (2)$$

Here ε_o is the imposed macroscopic deformation and $\varepsilon_{\text{local}}$ the local deformation.

A maximal value of $|\Delta\varepsilon|/\varepsilon_o = 80\%$ is measured and an average value of $|\Delta\varepsilon|/\varepsilon_o = 50\%$, 30%, and 30% respectively for 30%, 60%, and 90% of macroscopic strain. In addition, between 30% and 60%, it can be seen that some zone behaviors cross the continuous line. When the deformation of a zone (initially lower than the macroscopic one) crosses the line, one can suppose that its stiffness decreases to a value inferior than the average stiffness of the material. More curiously, some crossings in the other sense can be seen.

A model for quantitative analysis of strain heterogeneities in filled rubber has been proposed by Burr et al.,[30] which could explain these heterogeneities. Here, to describe qualitatively the heterogeneous behavior of the filled rubber we have preferred more simple model based on the same kind of ideas. This model is based on the superposition of several springs. In our case the aim is only to describe qualitatively the macroscopic behavior so that only four springs are used in the model (Figure 6). For each spring the constitutive law is given by $F_i = K_i\varepsilon_i$, where F_i is the force applied on the considered spring, K_i its stiffness, and ε_i the corresponding deformation.

The values of the different springs are arbitrary chosen to represent the experimental behavior (in this case $K_1 = 5$, $K_2 = 40$, $K_3 = 35$, and $K_4 = 60$). The displacement is imposed so that a strain of 100% is obtained.

Globally the experimental trends are reproduced, when the imposed macroscopic strain increases (Figure 6a), the difference between local and imposed (or macroscopic) strain increases. The K_i values have been chosen so that an average value of $|\Delta\varepsilon|/\varepsilon_o = 50\%$ is reached for any imposed deformation. To obtain such a results very different springs can be used, for example $K_4/K_1 = 12$. Even if this is a very simple model, this result let us suppose that very strong modulus heterogeneities can exist in the material leading only to an $|\Delta\varepsilon|/\varepsilon_o$ ratio of 50%. In Figure 6b, when the imposed strain reaches 30%, the stiffness of K_4 is decreased to 10 to mimic a fracture in the filler network. As expected, the strain for K_4 increases strongly, but in the same time, the strain for K_3 (same branch) decreases strongly.

It seems that the hypothesis of multiple springs in parallel and series coupling can explain qualitatively well the experimental behavior of the material. In particular, it is not necessary that the stiffness of a zone increases to provoke a strong decrease of its deformation. The cross in both senses is then likely determined by filler network fracture.

Filler Network Behavior in the Axial Direction. Self-Similarities in Strain Heterogeneities. Do the heterogeneities depend on the aggregates size? Or are they invariant whatever the scale as it is suggested by the fractal microstructure? To bring an answer to these questions, the initial aggregate size has to be taken into account in relation with the intensity of strain heterogeneities. In addition, the influence of the first and the second loading on strain heterogeneities is evaluated.

This kind of measurements has been performed on a large range of characteristic sizes (from around 50 to 2000 nm) on about 50 different zones and during the first and the second loading cycle. In addition, in order to obtain the same kind of information at significantly higher scale (from around 2 to 130 μm), the optic microscope of the AFM device has been used. In this case, topological incidents are chosen and their

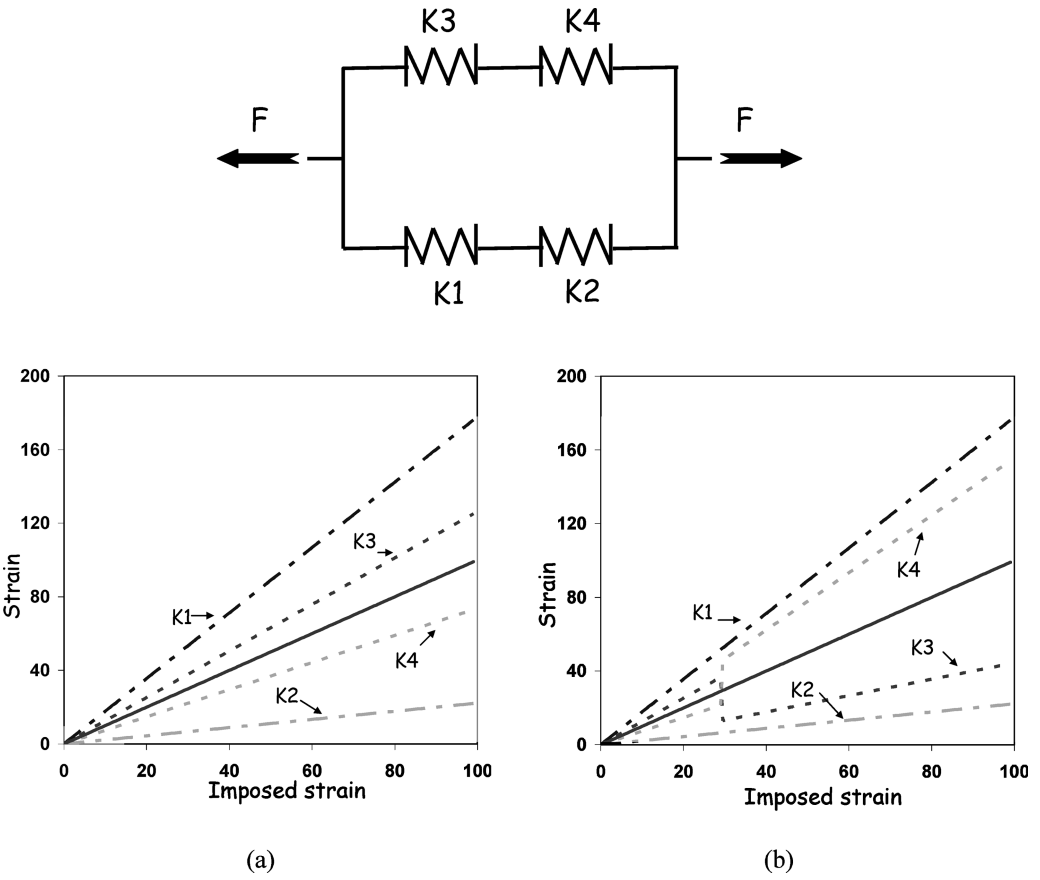

Figure 6. Schematic representation of the spring model (top), results obtained for different spring stiffness (a) and results obtained by "breaking" of one of the springs (b).

local elongations compared to the macroscopic one are reported. The main results are summed up in Figures 7 for first loading and 8 for second loading. On these figures $|\Delta\varepsilon|/\varepsilon_o$ is represented versus the imposed macroscopic strain and the initial size (or the characteristic size) of the aggregates (measured in nm or in μm).

Thanks to these representations, the overall evolution of strain heterogeneities can be examined on a very large characteristics size (from 50 nm to 130 μm). First of all, as suggested previously the intensity of heterogeneities seems to decrease slightly with the imposed deformation whatever the characteristic size. This effect could be the consequence of filler network fractures leading to a global homogenization of the local stiffness.

The most important information which can be obtained from these graphs is that 3 main regimes can be seen whatever the macroscopic strain imposed:

- From characteristic sizes between 30 to 800 nm, strong heterogeneities appear. The intensity of these heterogeneities seems to be invariant with the characteristic size.
- From characteristic sizes between 800 to 2000 nm, strain heterogeneities seem to decrease slightly. Again on this size range, strain heterogeneities seem to be invariant.
- From 2 to 100 μm strain heterogeneities reduce progressively and disappear.

From around 50 nm to 1 μm, the strain heterogeneities seem to be invariant which would be compatible with the fractal vision of the microstructure that is generally assumed. The maximal size of aggregate which would be similar to the smaller ones would be close to 1 μm. From 1 to 100 μm the heterogeneity decreases slowly to reach the homogeneous behavior. Even in considering the possible uncertainties on these measurements, it is clear that the deformation of a filled rubber with 15 phr of carbon black cannot be considered as homogeneous before a size of at least 50 μm.

During the second loading, the same experiments have been performed on the same zones. Qualitatively the same results are observed. Indeed, the strain heterogeneities decreases with the imposed deformation, and three regimes appear:

- From characteristic sizes between 50 to 1000 nm, strain heterogeneities are invariant.
- From characteristic sizes between 1000 to 2000 nm, strain heterogeneities are a little smaller.
- From 2 to 100 μm strain heterogeneities reduce progressively and disappear.

Globally, by taking into account the average values; it seems that the second loading is more heterogeneous than the first nearly until the return of the homogeneous behavior. Interestingly, it appears that the three same regimes can be observed comparing the first and the second loading. The Mullins effect characterized by a strong mechanical behavior difference (see Figure 1) could be, in part, explained by these behavioral differences. These observations are also compatible with the micromechanisms generally taken into account to predict Mullins effect.[31]

Rubber Incompressibility. As we have seen in the last sections, strain is strongly heterogeneous at local scale. For sure, it is heterogeneous in others directions than tension direction. As filled rubbers are well-known to be nearly

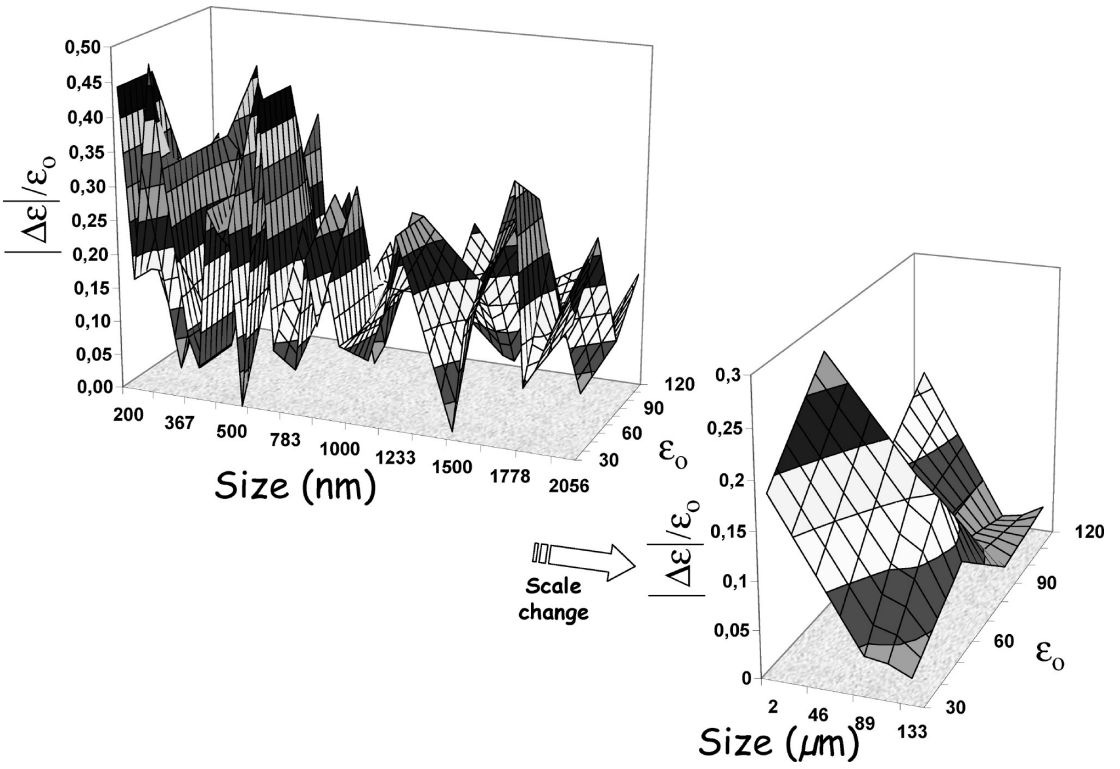

Figure 7. $|\Delta\varepsilon|/\varepsilon_o$ during a first loading cycle is represented versus the initial distance between aggregate and the macroscopic deformation. On the left are presented the results coming from AFM and on the right the results from optic microscopy.

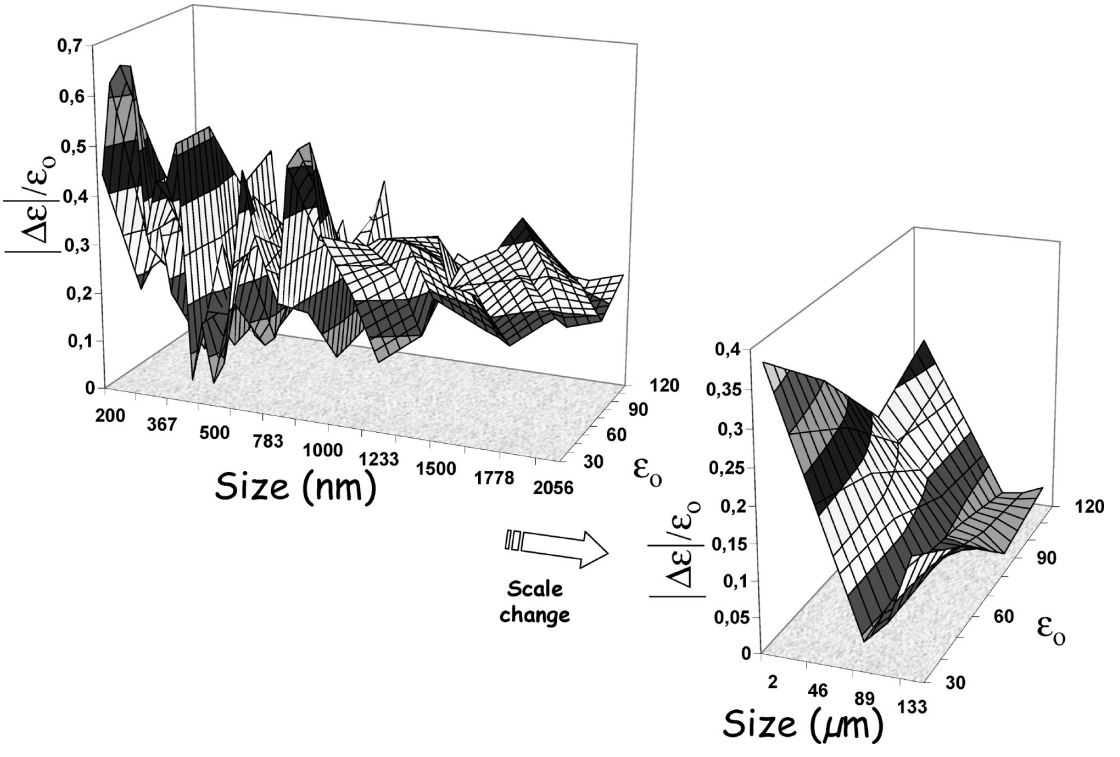

Figure 8. $|\Delta\varepsilon|/\varepsilon_o$ during a second loading cycle is represented versus the initial distance between aggregate and the macroscopic deformation. On the left are presented the results coming from AFM and on the right the results from optic microscopy.

incompressible, the question of the compatibility of the heterogeneous local strain field with an incompressible behavior is put forward. To answer this question, Strain measurements have been performed in all the directions of the surface of the sample. The displacement can be now defined as a vector. In Figures 9 and 10 are represented the evolution of the microstructure between 0 and 120% of imposed macroscopic strain respectively for the first and the second loading. The tensile direction is horizontal and the arrows indicate the chosen aggregates which are followed along the deformation. Moreover a grid is drawn to visualize the deformation.

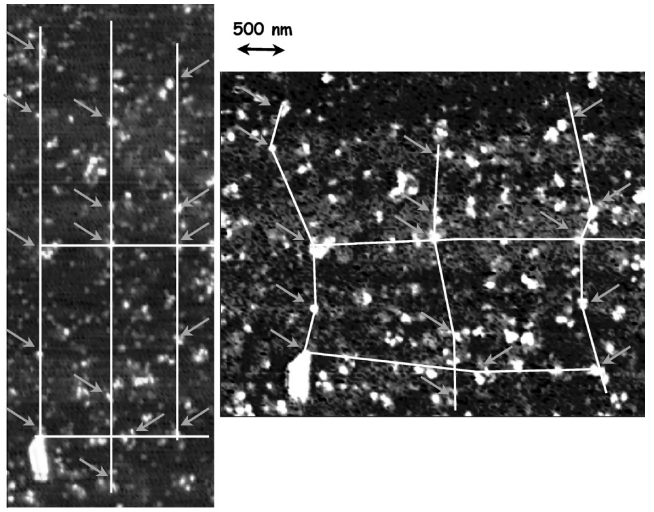

Figure 9. Local evolution of the microstructure along deformation (0 to 120%) and shape changes during first loading.

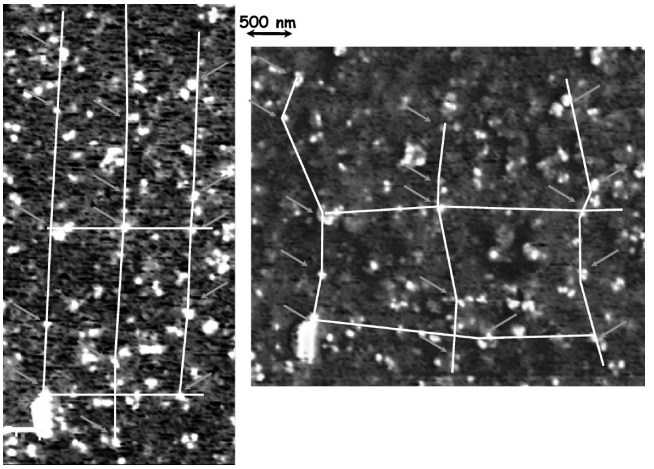

Figure 10. Local evolution of the microstructure along deformation (0 to 120%) and shape changes during second loading.

As described previously, during the first loading strain heterogeneities appear. The grid is then stretched but also deformed. The shape changes of the grid prove that some local shear or rotation occur as corollary phenomena to strain heterogeneities. After unloading (first image of Figure 10), the initial shape of the grid is nearly recovered which indicates that the deformation is quasi reversible (but not completely) even if the AFM phase contrast is different. During the second loading, the distortions of the grid are also similar to the ones observed during the first loading. The displacement differences between the first and second loading are difficult to measure and are close to the uncertainties. It seems that no major differences are visible at this scale between the first and the second loading.

Concerning the movements of the filler and their compatibility with the incompressibility of the filled rubber, it is proposed to compare the theoretical current lines for an incompressible fluid under axial elongation to the movement of aggregates (Figure 11). This study has been restrained on the second loading. On this figure, the incompressible current lines are represented with dotted line, the square is the reference from which the displacements have been measured: practically an aggregate has been chosen has a reference. Each arrow corresponds to the displacement of an aggregate during an imposed deformation step. The four consecutive

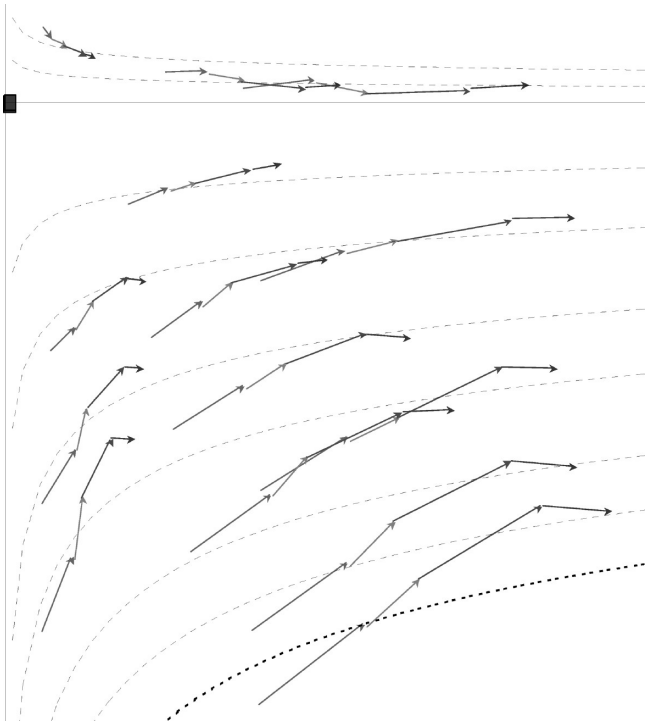

Figure 11. Comparison of local movements of fillers with current lines for an incompressible material.

arrows correspond to the movement of an aggregate for 30, 60, 90, and 120% of imposed strain. Fourteen aggregates have been followed along the second loading sequence.

From a step of elongation to the following, some aggregates follow approximately the theoretical current lines and others do not. On this measurement, it seems that most of the aggregates follow a movement notably different from an incompressible fluid during the first three loading sequences. During the last an adjustment seems to occur to approach the incompressibility. When an aggregate trajectory is to far from the average movement, it is likely that strong correction forces appear to reduce the deviations. A competition between the rubber flow (incompressible) and the filler network fracture leads to these perturbed trajectories. The deviation of the observed zone from an incompressible fluid can also be balanced by other zones of the material to maintain the overall incompressibility.

Finally, it appears clearly that the strong local strain heterogeneities and the deviations from the incompressible flow are not incompatible with the global incompressibility of the material.

Conclusion

In this study, we have used AFM tapping mode imaging to analyze local movements of carbon-black filler in a SBR rubber during tensile test. Low filler rate has been chosen to 15 phr. AFM is only a surface analysis technique; however the comparison between macroscopic displacement and microscopic ones is possible. By following the movements of several aggregates at various scales, it has been shown that the local strain is strongly heterogeneous and reaches a relative difference of 50% for initial aggregate sizes about 50 to 1000 nm. This result is the same for the first and the second loading sequence. At this observation scale, the heterogeneities seem to be invariant with initial aggregate size so that the microstructure as the deformation could be considered as fractal until around 1 μm. After 1 μm the strain heterogeneities decrease and reach progressively the homogeneous behavior for a size between 50 to 100 μm.

Along the loading sequence from 30 to 120%, some aggregates first deform less than the overall medium and more at the end. We have shown that it can be attributed to local fracture in the filler network. This effect, generally considered as the main cause for Payne effect, has been followed in situ along the deformation.

Macroscopically, Mullins effect has a strong influence on mechanical behavior as the stress for a given deformation as well as the dissipated energy is strongly higher compared to the following tensile loading sequences. This significant phenomenon does not lead to complete modification of the strain heterogeneities as the three same regimes are observed when comparing the first and second loading sequence. However, during the second loading the strain heterogeneities have appeared to be considerably higher than during the first for scale length between 1 to 50 μm. This observation is compatible with the classical mechanisms assumed for Mullins effect. Indeed, if some links between fillers are broken during the first loading, it could lead to an increase of the local strain heterogeneity.

In addition, local movements of aggregates have to accommodate the rubber flow which is incompressible. It has been shown that the aggregates follow partially this movement, when the deviation is too high, correction movements appear which could be correlated with filler network breakage. Consequently, each different aggregate is submitted to strong distortions to accommodate the continuity of the displacement field. Of course, little cavitations probably participate also.

Finally, all these experimental measurements have also shown that during a tensile test a filled rubber is submitted to opposite constraints. The rubber behaves as an incompressible medium carting partially the filler network. The filler network exhibits a rigid behavior that breaks only when the local stress reaches a threshold. Depending on the observed characteristic the behavior is either determined by the rubber behavior (incompressibility) or by the filler network (local heterogeneous deformation).

Acknowledgment. I would like to thank Morgane Belloir for the time spent at following and measuring trajectories of aggregates on the numerous AFM images.

References and Notes

(1) Boonstra, B. B. *Polymer* **1979**, *20*, 691–703.
(2) Kraus, G. *Rubber Chem. Technol.* **1978**, *51*, 297321.
(3) Suzuki, N.; Ito, M.; Yatsuyanagi, F. *Polymer* **2005**, *46*, 193–201.
(4) Wang, M. J. *Rubber Chem. Technol.* **1997**, 520586.
(5) Heinrich, G.; Kluppel, M. *Adv. Polym. Sci.* **2002**, *160*, 1–44.
(6) Meier, J. G.; Kluppel, M. *Macromol. Mater. Eng.* **2008**, *293*, 12–38.
(7) Koga, T.; Hashimoto, T.; Takenaka, M.; Aizawa, K.; Amino, N.; Nakamura, O. M.; Yamaguchi, D.; Koizumi, S. *Macromolecules* **2008**, *41*, 453464.
(8) Mélé, P.; Marceau, S.; Brown, D.; De Puydt, Y.; Alberola, N. D. *Polymer* **2002**, *43*, 5577–5586.
(9) Meier, J. G.; Mani, J. W.; Kluppel, M. *Phys. Rev. B* **2007**, *75*, 054202.
(10) Payne, A. R. *J. Appl. Polym. Sci.* **1962**, *6*, 368.
(11) Payne, A. R. *J. Appl. Polym. Sci.* **1963**, *7*, 873.
(12) Mullins, L. *Rubber Chem. Technol.* **1969**, *42*, 339–362.
(13) Bueche, F. *J. Appl. Polym. Sci. 5* **1960**, *10*, 107–114.
(14) Bueche, F. *J. Appl. Polym. Sci. 5* **1961**, *15*, 271–281.
(15) Ramier, J.; Gauthier, C.; Chazeau, L.; Stelandre, L.; Guy, L. *J. Polym. Sci.* **2007**, *45*, 286–298.
(16) Frohlich, J. W.; Niedermeier, H.-D. *Luginsland Composites: Part A* **2005**, *36*, 449–460.
(17) Kluppel, M.; Schuster, R. H.; Heinrich, G. *Rubber Chem. Technol.* **1997**, *70*, 243.
(18) Galuska, A. A.; Poulter, R. R.; McElrath, K. O. *Surf. Interface Anal.* **1997**, *25*, 418–429.
(19) Clément, F.; Lapra, A.; Bokobza, L.; Monnerie, L.; Ménez, P. *Polymer* **2001**, *42*, 6259–6270.
(20) Huy, T. A.; Adhikari, R.; Michler, G. H. *Polymer* **2003**, *44*, 1247–1257.
(21) Magonov, S. N.; Elings, V.; Whangbo, M. H. *Surf. Sci.* **1997**, *375*, L385–L391.
(22) Kopp-Marsaudon, S.; Leclère, Ph.; Dubourg, F.; Lazzaroni, R.; Aimé, J. P. *Langmuir* **2000**, *16*, 8432–8437.
(23) Brandsch, R.; Bar, G.; Whangbo, M. H. *Langmuir* **1997**, *13*, 6349–6353.
(24) Bar, G.; Brandsch, R.; Whangbo, M. H. *Langmuir* **1998**, *14*, 7343–7348.
(25) Bar, G.; Ganter, M.; Brandsch, R.; Delineau, L.; Whangbo, M. H. *Langmuir* **2000**, *16*, 5702–5711.
(26) Lapra, A.; Clément, E.; Bokobza; Monnerie, L. *Rubber Chem. Technol.* **2003**, *76*, 60–81.
(27) Christenson, E. M. Anderson, J. M. Hiltner, A. Baer, E. Source: *Polymer* **2005**, *46*, 11744−11754.
(28) Roland, C. M.; Robertson, C. G.; Nikiel, L.; Puskas, J. E. *Rubber Chem. Technol.* **2004**, *77*, 372–379.
(29) Lapra, A. *Etude des mécanismes de renforcement dans les réseaux d'élastomères chargés à la silice*; Ph.D. Thesis, Univ. Paris 6, 1999.
(30) Burr, A.; Monnerie, L. *Polymer* **2000**, *41*, 5909–5919.
(31) Markmann, G.; Verron, E.; Gornet, L.; Chagnon, G.; Charrier, P.; Fort, P. *J. Mech. Phys. Solids* **2002**, *20*, 2011–2028.